Effect of the Metal–Insulator Transition on the Thermoelectric Properties of Composites Based on Bi0.5Sb1.5Te3 with VO2 Nanoparticles

Santiago Alvarez-Guerrero, Jose Ordonez-Miranda, Romeo de Coss, Juan Jose Alvarado-Gil

Effect of the metal-insulator transition on the thermoelectric properties of composites based on $Bi_{0.5}Sb_{1.5}Te_3$ with VO_2 nanoparticles

Santiago Alvarez-Guerrero [1], Jose Ordonez-Miranda [2,3,*], Romeo de Coss [1] and Juan Jose Alvarado-Gil [1]

[1] *Departamento de Física Aplicada, Centro de Investigación y de Estudios Avanzados del I.P.N-Unidad Mérida, Carretera Antigua a Progreso km. 6, A.P. 73 Cordemex, Mérida, Yucatán 97310, México.*
[2] *LIMMS, CNRS-IIS UMI 2820, The University of Tokyo, Tokyo 153-8505, Japan.*
[3] *Institute of Industrial Science, The University of Tokyo, Tokyo 153-8505, Japan.*

[*] *Corresponding author: ordonez@iis.u-tokyo.ac.jp*

Abstract

Bismuth telluride–based materials have been widely investigated due to their applications for the development of high-performance thermoelectric devices. Here, we numerically determine the effective electrical conductivity (σ_{eff}), thermal conductivity (k_{eff}), and Seebeck coefficient (S_{eff}) of composite materials made up of VO_2 nanoparticles embedded in a $Bi_{0.5}Sb_{1.5}Te_3$ (BST) matrix. The temperature evolution of these three properties along with the thermoelectric figure of merit ($ZT = \sigma_{eff}S_{eff}^2T/k_{eff}$) is analyzed across the metal-insulator transition of VO_2 and for temperatures up to 550 K. For temperatures higher than 350 K, it is shown that VO_2 nanoparticles with a concentration of 34% enhance the electrical conductivity and *ZT* of the matrix by about 16% and 10%, respectively, while the Seebeck coefficient remains pretty much constant. This indicates that VO_2 nanoparticles provide an effective way to enhance the thermoelectric efficiency of $Bi_{0.5}Sb_{1.5}Te_3$ materials. The calculated *ZT* values for VO_2 are in good agreement with the experimental data reported in the literature for temperatures higher than 350 K. The thermal conductivity values obtained for VO_2 in the insulating phase are in good agreement with the experimental data reported in the literature, which are used to calculate the interface thermal resistance between $Bi_{0.5}Sb_{1.5}Te_3$ and VO_2. Furthermore, the ratio $k_{eff}/T\sigma_{eff}$ is found to be higher than the Lorenz number obtained for pure metals, such that its values increase with temperature and the VO_2 concentration, for temperatures higher than the transition temperature (342.5 K) of VO_2.

Keywords: Vanadium dioxide nanoparticles, Vanadium dioxide composites, Thermoelectric figure of merit.

1 Introduction

Thermoelectric (TE) materials enable direct and reversible heat-into-electricity conversion, for constituting the basis for green and environment-friendly energy technology.[1] Bi_2Te_3-based materials are known as narrow-gap semiconductors, with a bandgap of about 0.13 eV.[2] These compounds give rise to bipolar thermal conduction (k_b) at high temperatures which contributes to the total thermal conductivity according to the equation:

$$k = k_e + k_l + k_b, \quad (1)$$

where k_e and k_l are the electronic and lattice thermal conductivity, respectively. The increase in thermal conductivity leads to a poor thermoelectric efficiency. The efficiency of TE materials is determined by the dimensionless figure of merit $ZT = S^2\sigma T/\kappa$, where S is the Seebeck coefficient, σ is the electrical conductivity, T is the average temperature, and κ is the thermal conductivity. Unfortunately, these parameters are interdependent, improving one of them generally unbalances or diminishes the others, resulting in a limited energy-conversion efficiency.[3] Considerable effort has been devoted to improving the thermoelectric properties and overcome this challenge.

There are currently several methods for improving the performance of thermoelectric materials which are related to quantum approaches known as band engineering and phonon engineering. The pillars of these theories were established by Dresselhaus and Hicks in the early 1990s. They proposed the idea of size quantization with the possibility of improving the thermoelectric properties of materials.[4,5] Dresselhaus suggested the use of low dimensionality for decreasing the phonon thermal conductivity and increasing the product S^2n, where n is the charge carrier concentration. Dresselhaus and Hicks[4] continued this idea and calculated *ZT* values for a two-dimensional thin film. Their results showed that the 2D structure had an enhanced *ZT* coefficient compared with the 3D system of the same material. Following the same line of investigation, they also calculated *ZT* values for a quantum wire (1D) and confirmed that the corresponding *ZT* values for the one-dimensional system were enhanced with respect to the 2D quantum well.[5] In brief, they demonstrated that the nanostructures confine the electron wavefunction in one or two dimensions improving the thermoelectric efficiency. Therefore, size quantization acts on electrons and enables the so-called band structure engineering that is ascribed to the change in the density of states. The phonon engineering is related to obtain a reduced phonon mean free path in the material by means of interface scattering and hence a reduction in the lattice thermal conductivity.[5,6] For the case of a material in which k_l of Eq. 1 may be negligible, it could reach the upper limit of thermoelectric efficiency. [7]

The fundamentals of the enhancement of Seebeck coefficient by means of an increase in the density of states (DOS) establishes that the valence or conduction band of the host semiconductor resonates with one energy level of a localized atom in a semiconductor matrix.[8] Additionality, we can find alternative methods to boost the Seebeck coefficient that may include, enhancement of Seebeck coefficient by carrier energy effects,[9,10] inhibition of the intrinsic excitation effect,[11] or by embedding superparamagnetic nanoparticles into p-type matrices to improve the thermoelectric performance,[12] among other approaches.

There are interesting reports on the thermoelectric properties of different composite materials based on the $Bi_{0.5}Sb_{1.5}Te_3$ matrix,[10–12] for instance, Kim *et al.*[10] reported an enhancement of Seebeck coefficient in $Bi_{0:5}Sb_{1:5}Te_3$ with high-density tellurium nanoinclusions. They reported

experimental evidence that the addition of Te nanoparticles enhances the electron scattering by the carrier energy filtering effect due to the barrier potential formed by the Te/$Bi_{0:5}Sb_{1:5}Te_3$ interfaces. It was found that the addition of 15% in volume of tellurium into the $Bi_{0:5}Sb_{1:5}Te_3$ films increases the Seebeck coefficient significantly by more than 45% at 320K. However, the electrical conductivity decreases with increasing density of Te nanoparticles throughout the temperature range of 320 to 520 K.

More recently, Zhu *et al.*[11] investigated the addition of Cu impurity into a BST matrix. According to these authors, Cu impurities induce an enhancement in the thermoelectric behavior with an *ZT* average value of 0.85 across the entire temperature range due to synergistic optimization of the electronic and thermal transport properties. This *ZT* value was larger than that of the BST matrix of 0.52.

The effect of introducing magnetic nanoparticles in BST has also been explored. Li *et al.*[12] demonstrated that introducing superparamagnetic nanoparticles is an effective approach to simultaneously enhance the thermoelectric and cooling performance of p-type BiSbTe-based alloys. The authors incorporated Fe_3O_4 nanoparticles into a commercial $Bi_{0.5}Sb_{1.5}Te_3$ matrix and found that this induces the enhancement of the Seebeck coefficient due to the carrier multiple scattering. It also induces a significant decrease in thermal conductivity due to the phonon scattering caused by magnetic moment fluctuations. The composite reached a maximum *ZT* corresponding to 32% higher than that of the matrix.

It is well known that thermoelectric properties of strongly correlated electron systems could contribute to the semiconductor to metal transition (SMT).[13] Vanadium dioxide (VO_2) is a strongly correlated oxide,[14] which shows a SMT close to room temperature, which induces remarkable changes in its structural, optical, and electrical properties. These characteristics have made vanadium dioxide the basis in the development of a great diversity of technological applications, such as temperature sensors,[15] energy storage media,[16] thermally-driven radiative diodes,[17] among others. However, VO_2 has received little attention in the field of thermoelectricity.[14]

Few applications for VO_2 in thermoelectricity has recently emerged.[18,19] Kosta *et al.*[18] studied VO_2 nanoparticles embedded into thermoelectric n-type $Mg_2Si_{0.888}Sn_{0.1}Sb_{0.012}$ alloy. They found that the addition of VO_2 nano inclusions provide an extra scattering for the low frequency phonons, in addition to that caused by the point defects and dislocations that appear during the ball milling process, which can scatter high/medium-frequency phonons. As consequence, the effective thermal conductivity diminishes and the *ZT* increases by 38%.

Back *et al.*[19] investigated the thermoelectric properties of MgO/VO_2 BST composites by extrinsic phase mixing of MgO and VO_2 nanoparticles in the BST matrix. It is important to note that BST is a narrow gap semiconductor and presents the bipolar diffusion effect, which represents a critical point to increase the performance of the semiconductor. As is known, when the energy gap of a material is small, some electrons can be thermally excited to the next higher energy band leaving the corresponding empty states (holes).[20] Consequently, the total thermal conductivity is enhanced according to Eq. 1. Thus, the authors found that MgO and VO_2 distribution in the BST effectively scatters phonons, inducing a significant reduction of thermal conductivity by

decreasing lattice and bipolar thermal conductivity. These phenomena allowed the enhancement of the *ZT* values for the MgO/VO_2 BST composites over a wide range of temperatures.

Inspired by the above-mentioned works[18,19] and the fact that vanadium dioxide shows a fully reversible first-order metal-to-insulator transition accompanied by a relatively little change in its thermal conductivity and an abrupt jump by nearly two orders of magnitude in its electrical conductivity on heating,[21] we have investigated the influence of VO_2 on the electrical conductivity, thermal conductivity and Seebeck effect for VO_2/BST composites. Recently, Jung *et al.*[22] obtained an analytical expression for the effective thermoelectric properties and dimensionless figure of merit of a composite considering interfacial resistance. The model was developed via the mean-field homogenization scheme called the Mori–Tanaka method. The results were validated against the Finite Element Methods (FEM) with good agreement for volume fraction of inhomogeneities up to 20%.

Recently, Qiu *et al.* [23] experimentally studied the thermal conductivity from mesoporous to macroporous SiOC ceramics. Their thermal conductivities were measured in freestanding samples using the 3ω technique, subsequently they employed three typical models (series, Maxwell-Eucken 1, and effective medium theory) assigning adequate weights to each model and combining them to derive an empirical formula for the thermal conductivity. In this work, we combine the Bruggeman scheme,[24] (considered as one of the most accurate for high filler volume fractions) with the accuracy of the finite element methods[25] to evaluate the thermal conductivity, electrical conductivity, and Seebeck coefficient for composites of three different vanadium dioxide concentrations.

2 Numerical methodology

The methodology for modeling the thermoelectric properties of particulate VO_2/BST composites by means of numerical simulations is presented in this section. This approach is based on the finite element method of a 3D model that consists of a set of spherical particles randomly distributed inside a cubic matrix. The spatial distribution of the inclusions is generated using a MATLAB™ code that ensures the non-overlapping of the inclusions, as detailed in our previous work.[26]

2.1 Effective electrical conductivity

A similar procedure to the one described by Nilsson *et al.*[27] was used to calculate the effective electrical conductivity. The cubic domain (matrix) with VO_2 inclusions is illustrated in Fig. 1(a). The bottom side of the domain was electrically grounded at 0 V (V_Γ = 0 V), a constant voltage was applied to the upper side (V_Γ = 1 V), whereas periodic boundary conditions were established on the remaining four sides ($V_{\Gamma a} = V_{\Gamma b}$). For the particles, the relationship describing the electrical conductivity of VO_2[24] as a function of temperature is as follows:

$$\sigma_{VO_2}(T) = \frac{(3f_m - 1)\sigma_m + (3f_i - 1)\sigma_i + \sqrt{((3f_m - 1)\sigma_m + (3f_i - 1)\sigma_i)^2 + 8\sigma_m\sigma_i}}{4}, \qquad (2)$$

where σ_m = 84175.1 Sm^{-1} and σ_i = 4.86 x 10^6 $e^{-3136.1/T}$ Sm^{-1} are the electrical conductivity in its dielectric (low temperature) and metallic (high temperature) phases, respectively; T_t = 3626.2 K is the transition temperature. f_m and f_i = 1 - f_m are the volume fractions of the metallic and insulating domains during the SMT, both are temperature dependent functions according to the equations:

$$f_m = -\frac{T}{U} W_0\left[-\frac{T}{2U}\exp\left(-\frac{T}{U}\right)\operatorname{erfc}\left(\frac{T_t - T}{\sqrt{2}\Delta T}\right)\right], \quad (3)$$

$$f_i = \frac{T}{U} W_0\left[-\frac{T}{2U}\exp\left(-\frac{T}{U}\right)\operatorname{erfc}\left(\frac{T - T_t}{\sqrt{2}\Delta T}\right)\right], \quad (4)$$

where U = 323.7 K is the activation energy, W_0 is the main branch of the Lambert W function, and ΔT = 5.5 K is the standard deviation for the heating process. The main branch of the Lambert function was implemented in MATLAB™ code and called as an external function from COMSOL™ software.

For the $Bi_{0.5}Sb_{1.5}Te_3$ material, the electrical conductivity values were taken from the experimental work reported by Li *et al.*[12] and implemented in COMSOL™ as the interpolation function "*sigma(T)*". The effective electrical conductivity was calculated by solving the Poisson equation with respect to the electric potential V, using a DC stationary method,[27]

$$\nabla.(\sigma \nabla V) = 0. \quad (5)$$

The magnitude of the effective electrical conductivity was obtained by integrating the current, $I = \sigma \nabla V$ over the whole cubic computational domain and dividing the result by the area, A of the grounded face and the applied voltage as follows,

$$\sigma_{eff} = \frac{I}{AV}. \quad (6)$$

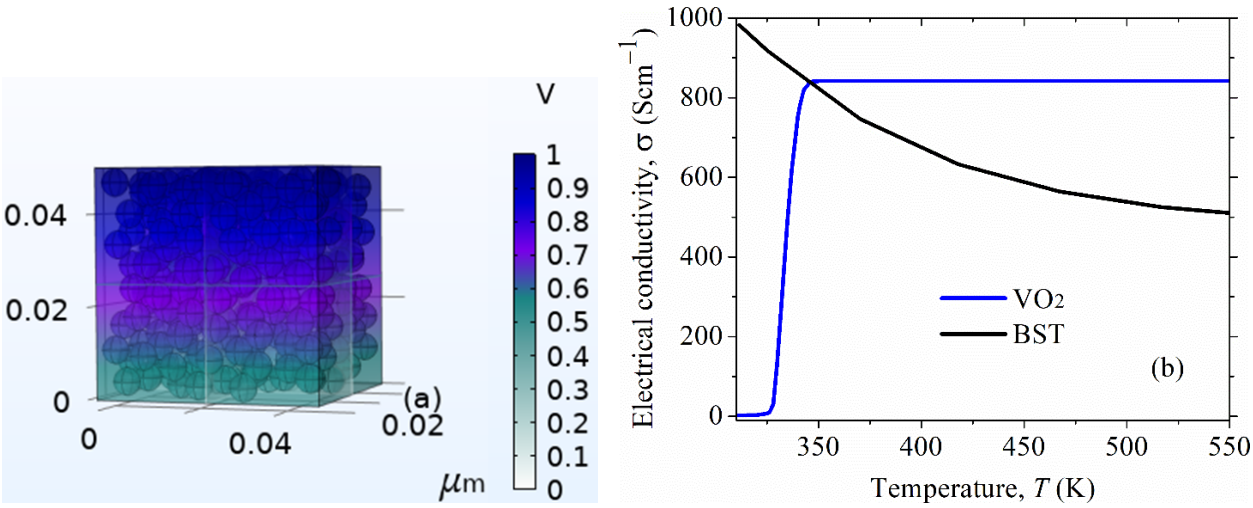

Figure 1. (a) 3D domain geometry to simulate the effective electrical conductivity. The colors indicate an electrical potential ranging from V = 1 V (blue zone) to V = 0 V (green zone). (b)

Temperature dependence of the electrical conductivity for the VO_2 (blue line) and for $Bi_{0.5}Sb_{1.5}Te_3$ (black line).

2.2 Effective thermal conductivity

The analytical function that describes the thermal conductivity of VO_2, $k_{VO_2}(T)$ can be reasonably well described as follows,[28]

$$k_{VO_2}(T) = k_d + \frac{k_m - k_d}{1 + e^{-\beta(T-T_c)}}, \quad (7)$$

where k_d = 3.6 $Wm^{-1}K^{-1}$ and k_m = 6.0 $Wm^{-1}K^{-1}$ are the thermal conductivity in its dielectric (low temperature) and metallic (high temperature) phases, respectively; T_c = 342.5 K is the transition temperature and β = 3.6 K^{-1} is the phase-transition slope of $k_{VO_2}(T)$ at $T = T_c$. For the $Bi_{0.5}Sb_{1.5}Te_3$ material, the thermal conductivity values were taken from the experimental data reported by Back *et al.*[19] and implemented in COMSOL™ as the interpolation function "*kappa(T)*". The effective thermal conductivity was calculated, solving the Fourier equation by means of the stationary method, as is described in our previous work.[26]

In the 3D model (see Fig. 2(a)), the top surface temperature (red zone) is kept higher than the bottom one (white zone) to induce a heat flux from top to bottom. All the remaining four surfaces are thermally insulated. The average value of conductive heat flux, normal to all three *xz* surfaces, is used to calculate the k_{eff} by means of the Fourier law of heat conduction,

$$\nabla.\left(k_{eff}T\right) = 0. \quad (8)$$

The heat flux q in the cubic domain was evaluated as the surface integration of the normal total heat flux in the top-to-bottom direction as follows,

$$q = \iint q_x(x,y,z)dydz, \quad (9)$$

and thus, the effective thermal conductivity, k_{eff}, is calculated as follows,

$$k_{eff} = \frac{q}{l(T_{hot} - T_{cold})}, \quad (10)$$

where l is the length of the cubic domain.

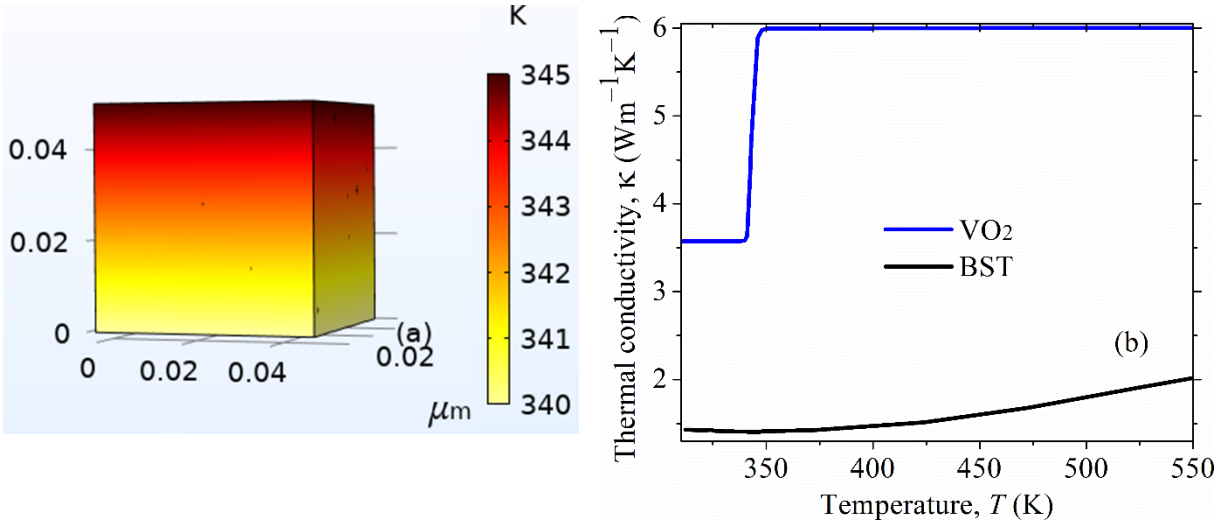

Figure 2. (a) Schematic representation of the 3D composite model. (b) Temperature dependence of the thermal conductivity of VO_2 (blue line) and for $Bi_{0.5}Sb_{1.5}Te_3$ (black line).

2.2.1 Calculation of the interface thermal resistance between VO_2 and $Bi_{0.5}Sb_{1.5}Te_3$

Interfacial thermal resistance is among the most relevant parameters determining the thermal conductivity of composites, and it is even present at atomically perfect interfaces. This resistance appears because of the physical differences, between neighboring materials, generating heat carriers scattering. These effects have been extensively explored in the literature and it has been shown that the numerical values appear in a broad range. This property has been specially studied in carbon nanostructures in which it has explored the determinant role of low frequency phonons. [29,30]

For our system made up with two different materials, we theoretically estimated the interfacial thermal resistance magnitude between VO_2 and $Bi_{0.5}Sb_{1.5}Te_3$ based on previous experiments. As we mentioned before, Back *et al.*[19] investigated the thermoelectric properties of VO_2/ $Bi_{0.5}Sb_{1.5}Te_3$ composites. They found that the dispersion of VO_2 particles effectively scatter the heat-carrying phonons resulting in a reduced thermal conductivity. The idea that the interfacial phonon scattering enhances the *ZT* figure of merit in thermoelectric materials was pointed out by Hicks and Dresselhaus.[5] According to their calculations, a significant increase in *ZT* can be achieved by going to lower dimensions,[5,6] particularly, a one-dimensional Bi_2Te_3 nanowire will undergo an increase in phonon scattering from the surfaces and this leads to a reduction in the lattice thermal conductivity.

The lattice thermal conductivity, k_l is related to the mean free path, λ according to the equation: $k_l = \frac{1}{3} C_v v \lambda$, whrere C_v is the lattice heat capacity and v is the sound velocity. We know from Ref. 19 that the mean free path is ~ 70 nm. Thus, if the diameter d of the particles is smaller than λ, the scattering at the surface will occur and cause a decrease in k_l.[5] Therefore, the total thermal conductivity is reduced with respect to the composite material. Based on this fact and assuming

that the quantization effects could be observed for nanostructures < 50 nm, we have considered a diameter for the spherical particles of d = 6 nm.

It is well known that the reduction of the effective thermal conductivity caused by the scattering of charge carriers is synonymous with the existence of interfacial thermal resistance. Phonon scattering mainly slants the heat transfer due to a barrier that is formed at the boundary interface yielding thermal boundary resistance (TBR). In addition, the less contact between fillers yields thermal contact resistance (TCR), which results in lower thermal conductivity. Therefore, the interfacial thermal resistance is a contribution of both TBR and TCR.[31] Different studies have experimentally reported the total thermal conductivity values for different vanadium dioxide samples. For thin films of VO_2, Kizuka *et al.*[32] reported that the total thermal conductivity increases from 3.6 to 5.4 $Wm^{-1}K^{-1}$. Oh *et al.*[33] reported an increase from 3.5 to 6 $Wm^{-1}K^{-1}$ in thin films of VO_2. Meanwhile Chen *et al.*[34] reported a decrease from 3.5 to 2.2 $Wm^{-1}K^{-1}$ for polycrystalline VO_2. The authors explain that this behavior of the thermal conductivity with temperature is caused by the reduction of the lattice thermal conductivity across the phase transition. Therefore, the differences in the variation trends of the thermal conductivity, reported in previous works, might be caused by discrepancies induced by the carrier contribution, which are sensitive to the structure and defects of the samples.

Therefore, according to abovementioned experimental data,[32–34] it can be inferred that whatever the sample, bulk or thin films, the thermal conductivity of VO_2 is ~3.6 $Wm^{-1}K^{-1}$ in the insulating phase. In the case under consideration in this work, we followed the results reported by Back *et al.*[19] These authors synthetized a composite mixing 15 g of $Bi_{0.5}Sb_{1.5}Te_3$ (m_{BST}) powder with 5 mol.% of VO_2 (n_{VO_2}) nanopowders. The volumetric composition, f for this composite was obtained using the equation:

$$f = \frac{100 n_{VO_2} M_{VO_2} \rho_{BST}}{n_{VO_2} M_{VO_2} \rho_{BST} + m_{BST} \rho_{VO_2}}. \quad (11)$$

From the density values for BST (ρ_{BST}) and for VO_2 (ρ_{VO_2}) and its corresponding molar mass (M_{VO_2}) values, we obtain the value f = 29.4% of VO_2. Then, the corresponding interfacial thermal resistance is calculated by fitting the experimental data and theoretically predicted effective thermal conductivity for an ITR value that matches in a temperature range in which VO_2 undergoes the insulating phase.

To carry out the simulations we considered a thin interface layer between both adjacent different materials (see Fig. 1(a)) where heat cannot flow directly through the layer which results in a temperature jump across the interface.[35] The interfacial thermal resistance, R is defined as

$$T^{out} - T^{in} = -R q_s . n, \quad (12)$$

where T^{out} and T^{in} refer to temperatures at the outer and inner surfaces of the interface, respectively, q_s is the heat flux at the interface, and the n is the outward surface normal vector. The results of this approach are shown in section 3.1.

2.3 Seebeck coefficient calculation

To know the overall effect of VO_2 on the $Bi_{0.5}Sb_{1.5}Te_3$ thermoelectric matrix, we have also determined the Seebeck coefficient for the $VO_2/Bi_{0.5}Sb_{1.5}Te_3$ composites. Seebeck coefficient (S) is a property of a material depending on its electronic structure near the Fermi level.[36] The sign of S indicates which charge carriers dominate the electronic transport in semiconductors as well as in metals. Negative values of S indicate that the material is an n-type semiconductor.

We simulated the Seebeck effect by means of a thermoelectric generator system implemented in COMSOL™. This system allows the Seebeck effect, a phenomenon where the difference in temperature of a material leads to a potential difference. We employed a brick-shaped domain with six sides as shown in Fig. 3(a). The thermoelectric part is made up of $Bi_{0.5}Sb_{1.5}Te_3$ and it is capped by two thin copper electrodes while the VO_2 spherical particles are embedded inside the matrix. To estimate the Seebeck coefficient magnitude, we employed the floating potential boundary condition to calculate the potential difference that undergoes the system. Then, we take the ratio of the potential difference or floating potential (that is the thermoelectric voltage seen at the Cu terminals) to the temperature difference as follows,

$$S_{eff} = -\frac{\Delta V}{\Delta T}. \tag{13}$$

A considerably large temperature difference was set on the surface of the electrodes, for example, 100 °C at the left of the boundary of the Cu electrode and 0 °C at the right of the Cu electrode. The relative permittivity values for VO_2 were taken from the experimental results reported by Yang *et al.*[37] and implemented in COMSOL™ as the piecewise function "$epsilon(T)$". Although the dielectric constant of the $Bi_{0.5}Sb_{1.5}Te_3$ matrix is unknown, it is likely lower than that of Sb_2Te_3 and probably near to 50.[38,39] The Seebeck coefficient values for VO_2 were taken from the work reported by Khan *et al.*[14] and implemented in COMSOL™ as the piecewise function "$Seebeck\_VO_2$". Meanwhile the corresponding Seebeck coefficient values for $Bi_{0.5}Sb_{1.5}Te_3$ material were taken from the experimental data reported by Back *et al.*[19] and implemented in COMSOL™ in the same way with the function "$Seebeck$_BST". Fig. 3(b) shows the Seebeck coefficient for both VO_2 and BST as a function of the temperature and in general, the properties employed to the simulations are detailed in Table 1.

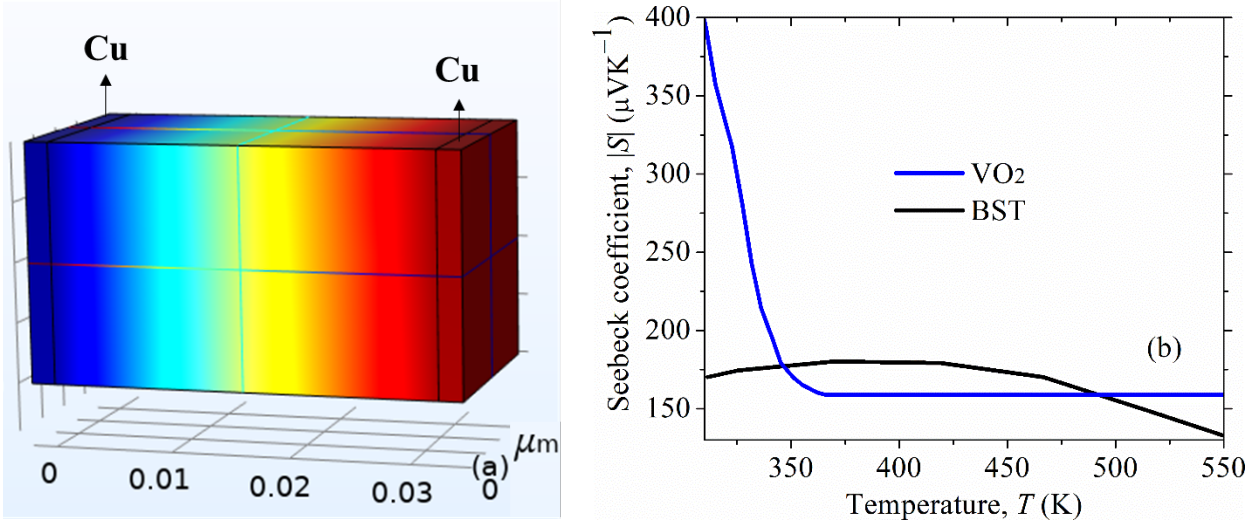

Figure 3. (a) Schematic representation of the modeled composite made up of a $Bi_{0.5}Sb_{1.5}Te_3$ matrix hosting in which particles of VO_2 nanoparticles. (b) Seebeck coefficient as a function of temperature of BST (black line) and VO_2 (blue line). The blue and red colors in (a) stand for the electrical potential applied to the composite material, blue (1 V) and red (ground potential).

Table 1. Electrical, thermal, and thermoelectric properties for the components of the $VO_2/Bi_{0.5}Sb_{1.5}Te_3$ composite.

Property	Cu electrodes	$Bi_{0.5}Sb_{1.5}Te_3$	VO_2
Relative permittivity	1	50	$epsilon(T)$
Electrical conductivity	5.998 x 10^7[S/m]	*sigma(T)*	Eq. 2
Heat capacity at constant pressure	385[J/(kg*K)]	185.9895[J/(kg*K)]	*
Density	8960[kg/(m*K)]	6840[kg/(m*K)]	4381.161-0.1409686*T
Thermal conductivity	400[W/(m*K)]	*kappa(T)*	Eq. 7
Seebeck coefficient	6.5 x 10^{-6} [V/K]	*Seebeck* $_{BST}$*(T)*	*Seebeck* $_{VO_2}$*(T)*

*We have previously developed a COMSOL™-readable heat capacity function for VO_2.[26]

3 Results and discussions

In this section we present the results of the simulations performed for the $VO_2/Bi_{0.5}Sb_{1.5}Te_3$ composites. It is important to mention that VO_2 are not participating as dopant (which means that vanadium dioxide does not change the crystallinity of the $Bi_{0.5}Sb_{1.5}Te_3$ matrix) and our simulations contemplate that VO_2 undergoes the "ideal efficiency" in its thermal conductivity (3.6 - 6.0 $Wm^{-1}K^{-1}$) and electrical conductivity (131 - 8.4 x 10^4 Sm^{-1}). To ensure the physical property calculations accuracy, in each case 3 repetitions were carried out, and the average results are reported as follows.

3.1 Electrical conductivity, thermal conductivity and Seebeck coefficient

First, we discuss the results for electrical conductivity. The temperature-dependent electrical conductivity for VO_2 nanoparticles embedded in $Bi_{0.5}Sb_{1.5}Te_3$ as a function of temperature is shown in Fig. 4. At low temperatures (< 350 K), the effective electrical conductivity tends to decrease, since VO_2 is still in the insulating phase and the conductivity of the BST decreases with increasing temperature (Fig. 1(b)). At about 327 K the curves reach a minimum, then the electrical conductivity starts to increase continuously with increasing temperature, ought to the changing of VO_2 into the metallic phase until reaching a maximum at ~348 K. It is interesting to note that this maximum value corresponds to the intersection of the conductivity curves of both VO_2 and BST as seen in Fig. 1(b). Thereafter, the curve decreases, but the EEC values are significantly higher than those of the BST matrix.

With the increasing of VO_2 concentration, the electrical conductivity enhances continuously. As the temperature increases, the electrical conductivity of $Bi_{0.5}Sb_{1.5}Te_3$ tends to ~500 Scm^{-1} meanwhile the effective electrical conductivity for the $VO_2/Bi_{0.5}Sb_{1.5}Te_3$ composite with f = 34.0% of VO_2 reached 625 Scm^{-1} at 550 K, which was around 16% greater than that of the BST matrix (525 Scm^{-1}) at the same temperature. This is relevant considering the range of temperature for thermoelectric applications (T < 1000 °C).

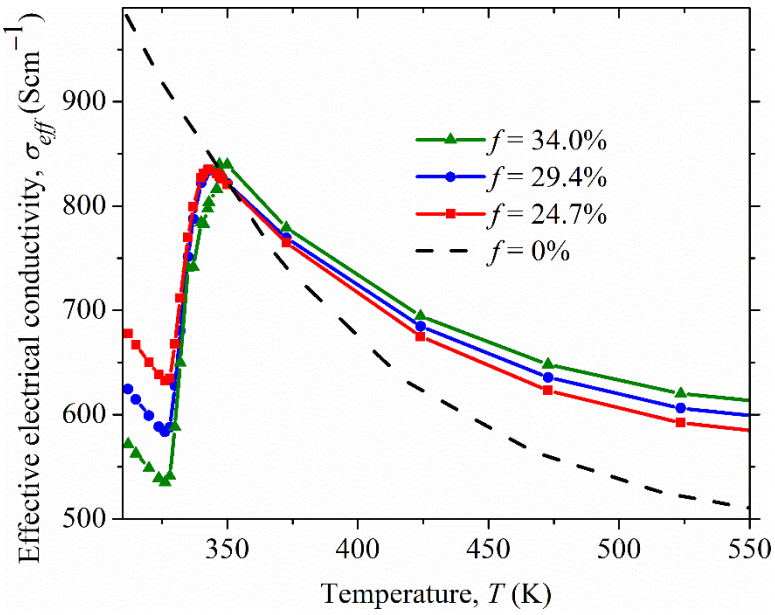

Figure 4. Temperature dependence of electrical conductivity for $VO_2/Bi_{0.5}Sb_{1.5}Te_3$ composites for different VO_2 concentration.

The improvement of the electrical conductivity could contribute to the direct enhancement of the thermoelectric efficiency in $Bi_{0.5}Sb_{1.5}Te_3$ bulk materials if the thermal conductivity is reduced or kept nearly constant.

Turning our attention to the effective thermal conductivity results. The ETC values as a function of temperature are plotted in Fig. 5. We tested various interface thermal resistance values until we obtained the blue curve depicted in Fig. 5(a), the inset in the figure shows a good agreement with the experimental results reported by Back *et al.*[19] within the temperature range for T < 350 K. Then, based on the methodology described in section 2.2.1, we estimated the interface thermal resistance between $Bi_{0.5}Sb_{1.5}Te_3$ and VO_2 as $R = 1.91$ m^2KGW^{-1}. This approximation is reasonable because the VO_2 nanoparticles yield large interfacial area and the interfaces among different phases have been shown to play an important role as phonon scattering centers.[39,40]

The calculated ETC values increase as the temperature increases, and at ~ 343 K a change in the slope of the curve is observed. In Fig. 5, it can be clearly observed the effect on the thermal conductivity of the VO_2 fraction undergoing the phase change from insulator to metal on heating. In other words, our results (blue curve in Fig. 5(a)) show the behavior for the $VO_2/Bi_{0.5}Sb_{1.5}Te_3$ composite if the VO_2 experiences what we have called the "ideal efficiency" on its thermal conductivity (3.6 - 6.0 $Wm^{-1}K^{-1}$). Although the magnitude of the thermal conductivity of VO_2 in the metallic phase is larger than the one for the matrix, the total ETC values for all concentrations of VO_2 are lower than that of the pure BST (see Fig. 5(b)), which is favorable for thermoelectric purposes.

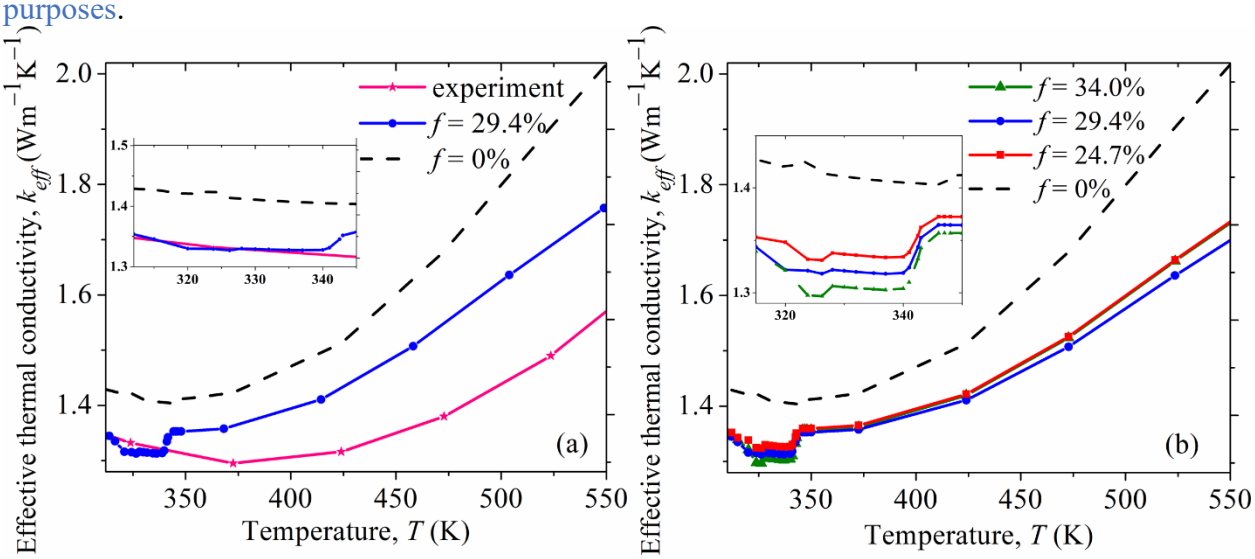

Figure 5. (a) The comparison between the theoretical effective thermal conductivity (blue line) predicted by the simulations and the experimental [19] results (pink line). (b) The effective thermal conductivity versus temperature calculated for various concentrations.

In the following, the results for the thermoelectric behavior of the $VO_2/Bi_{0.5}Sb_{1.5}Te_3$ are presented. We determined the Seebeck coefficient values, in which the simulated thermoelectric generator was tested at various temperature differences (ΔT), while the cold side was maintained at 0 °C. Fig. 6(a) portrays the variation of Seebeck coefficient (S) against temperature (T). Positive Seebeck coefficient values indicate the p-type conduction behavior. For low temperatures, the Seebeck coefficient values for the composite with f = 34.0% of VO_2 is slightly above the corresponding values of the matrix. This is due to the fact that in the semiconductor phase, VO_2 shows large values of S (see Fig. 3(b)) as a consequence of the significant enhance in the average energy of carriers, that takes part in transport phenomenon at low temperatures.[14] When the

temperature increases, the total Seebeck coefficient of the composites slightly decreases due to the dominant contribution of the matrix. In other words, the addition of VO_2 in the BST matrix does not improve the values of Seebeck coefficient. This can be explained as another consequence of the interface thermal resistance as follows: The Seebeck coefficient refers to the generated voltage difference for a given temperature difference through an electrical path. If a jump of the temperature occurs at the interface, the effective total temperature difference is reduced across the hot to cold side while the electrical current can flow through the inclusion. As a result, the thermoelectric composite produces less voltage as the interface thermal resistance increases.[22]

Notice that for T < 350 K, the Seebeck coefficient values for composites are slightly larger than those of the matrix. For T > 350 K, *S* slightly decreases with respect to the matrix. From this analysis we conclude that this thermoelectric property remains almost unchanged. Fig. 6(b) shows the dimensionless thermoelectric figure of merit (*ZT*) for pure BST and for the composites as function of temperature. It can be observed that *ZT* values of all composites increase with increasing temperature to reach a maximum value and then to decrease with further increase in temperature. Moreover, the *ZT* values significantly increased with the incorporation of VO_2 nanoparticles and it is notable that there is a good agreement between the experimentally determined *ZT* values and our calculations of $VO_2/Bi_{0.5}Sb_{1.5}Te_3$ composites for f = 29.4% VO_2. The low *ZT* values of composites at low temperatures is a consequence of changes that VO_2 undergoes for both thermal and electrical properties. Nevertheless, the composite with f = 34.0% exhibited a maximum *ZT* value of ~0.7 at 375 K, which is around 10% higher than that of BST matrix. On the other hand, Li-based ternary Heusler compounds reach its maximum TE efficiency of ~0.8 at about 200 K [41] which indicate that they can be adequate for cooling applications. In our case, considering the $VO_2/Bi_{0.5}Sb_{1.5}Te_3$ performance makes it suitable for room temperature or intermediate (350 – 450 K) applications.

From Fig. 6(b), it is also observed that for higher temperatures, the figure of merit values showed a significant improvement of around 20% compared with pure $Bi_{0.5}Sb_{1.5}Te_3$. Thus, this improvement is primarily due to the enhancement of the electrical conductivity and reduction in thermal conductivity. The trends of the *ZT* curves for the composites are similar to the Heusler quaternary compound PdZrTiAl, the metallic nature of this alloy in spin down leads to an acceptable extent amount of ZT in the entire temperature range, so it has the ability to use in power generators.[42] In our case, the $VO_2/Bi_{0.5}Sb_{1.5}Te_3$ composite material with a *ZT* range 0.8-0.3 may be suitable for waste heat utilization.[43]

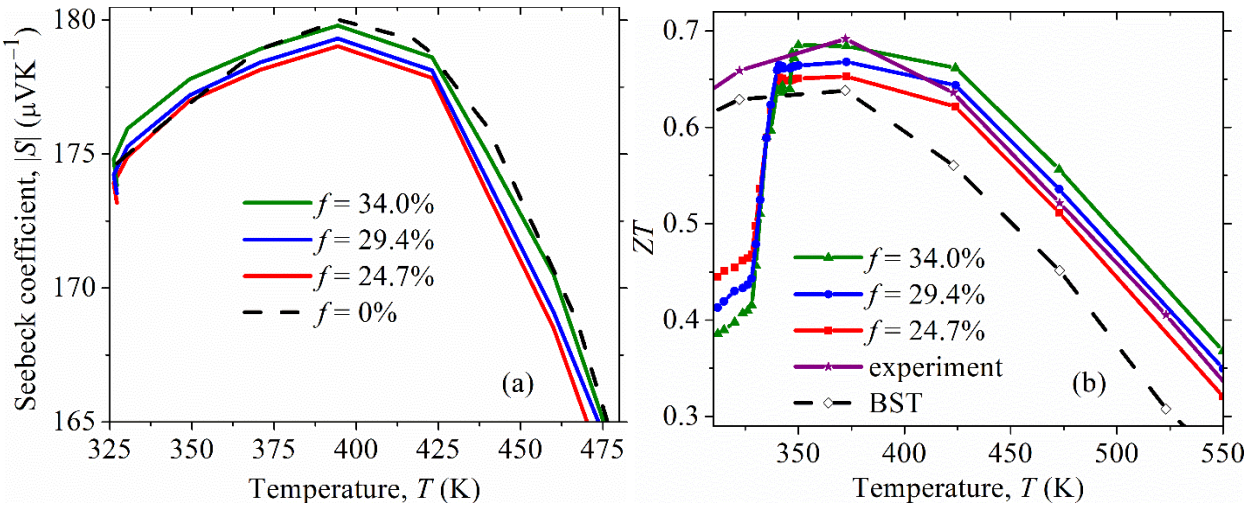

Figure 6. Thermoelectric properties of $VO_2/Bi_{0.5}Sb_{1.5}Te_3$ composite material as a function of temperature (a) Seebeck coefficient, (b) Figure of merit.

The improvement in the *ZT* values of BST matrix is due to the reduction in the thermal conductivity and the remarkable increase in the electrical conductivity compensating for the slight decrease of Seebeck coefficient caused by the addition of VO_2 nanoparticles. Experimentally, it has been also reported that the embedding of nanoparticles in BST matrix significantly enhances the thermoelectric performance.[44]

3.2 Relationship between thermal conductivity, electrical conductivity, and temperature

The relationship between the thermal conductivity and the electrical conductivity is established by the Wiedemann–Franz (WF) law. This law was originally developed for metals based upon the fact that heat and electrical transport both involve the free electrons. The law states that the ratio of the electronic contribution of the thermal conductivity to the electrical conductivity of a metal is proportional to the temperature according to the following relationship,

$$\frac{\kappa}{\sigma} = LT, \tag{14}$$

where L is the constant of proportionality known as Lorenz number.[45] For metals, this constant is denoted as L_0 and its value is equal to 2.45×10^{-8} $WS^{-1}K^{-2}$. For pure materials, the values of L are also well known. However, for alloys or composite materials this value is unknown.

Here, it is noteworthy that due to the correlated nature of VO_2 it is not allowed to calculate the expected electronic thermal conductivity, using the Wiedemann-Franz approach for the entire range of temperatures. [46,47] The relationship between the conductivities and temperature is quantified in Fig. 7. It is seen how the values of $\kappa/T\sigma$ for composites are lower than those of the matrix. In addition, for all concentration the corresponding values are slightly higher than L_0, which can be helpful in evaluating the role of electrons as energy carriers in these systems.

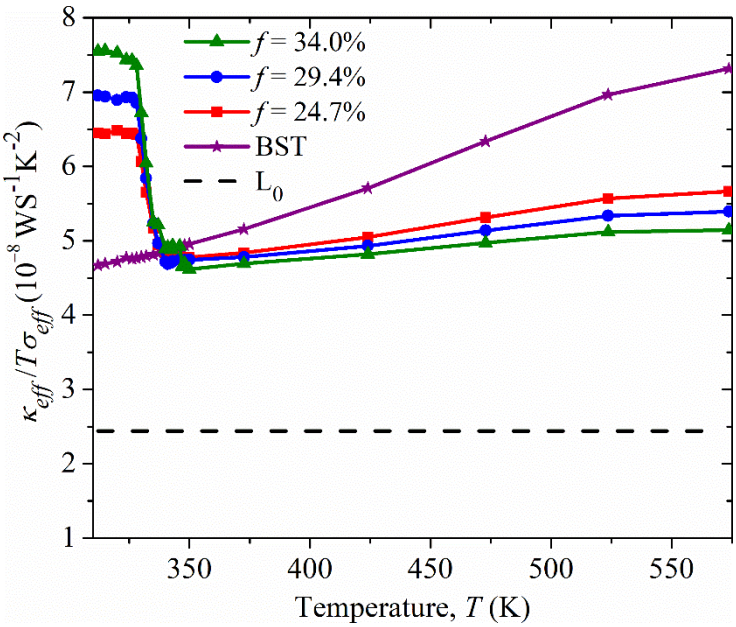

Figure 7. Temperature dependence of $\kappa/T\sigma$ relation for $VO_2/Bi_{0.5}Sb_{1.5}Te_3$ composite as temperature function.

4 Conclusions

The thermoelectric properties of $VO_2/Bi_{0.5}Sb_{1.5}Te_3$ composites with volume fractions of 0, 24.7%, 29.4% and 34.0% have been investigated across the metal-insulator transition of VO_2 and for temperatures up to 550 K, by means of simulations based on Finite Element Methods. We have shown that VO_2 nanoparticles with a concentration of 34.0% enhance the electrical conductivity by approximately 16% for temperatures higher than 350 K, while the Seebeck coefficient remains pretty much constant. The resulting maximum value of ZT = 0.7 shows up at 375 K, which represents an increase of 10% in comparison with the corresponding one of the matrix. The calculated ZT values agree well with experimental data and indicate that VO_2 nanoparticles provide an effective way to enhance the thermoelectric efficiency of $Bi_{0.5}Sb_{1.5}Te_3$ materials. We have estimated the interface thermal resistance magnitude between $Bi_{0.5}Sb_{1.5}Te_3$ and VO_2 as R = 1.91 m^2KGW^{-1}. Furthermore, it has been found that the ratio $k_{eff}/T\sigma_{eff}$ is higher than the Lorenz number obtained for pure metals, such that its values increase with temperature and the VO_2 concentration, for temperatures higher than the transition temperature (342.5 K) of VO_2. Finally, we want to emphasize that the numerical approach presented here can be useful to predict the effective thermoelectric properties of composites based on VO_2.

Availability of data:
The data that support the findings of this study are available from the corresponding author upon reasonable request.

References

1. L. E. Bell, Science. **321**, 1457 (2008).
2. I. G. Austin, Proc. Phys. Soc. **72**, 545 (1958).
3. Z.-H. Ge, X. Chong, D. Feng, Y.-X. Zhang, Y. Qiu, L. Xie, P.-W. Guan, J. Feng, and J. He, Mater. Today Phys. **8**, 71 (2019).
4. L. D. Hicks and M. S. Dresselhaus, Phys. Rev. B **47**, 12727 (1993).
5. L. D. Hicks and M. S. Dresselhaus, Phys. Rev. B **47**, 16631 (1993).
6. J. P. Heremans, M. S. Dresselhaus, L. E. Bell, and D. T. Morelli, Nat. Nanotechnol. **8**, 471 (2013).
7. M. Yeganeh, F. Kafi, and A. Boochani, Superlattices Microstruct. **138**, 106367 (2020).
8. G. D. Mahan and J. O. Sofo, Proc. Natl. Acad. Sci. **93**, 7436 (1996).
9. S. V Faleev and F. Léonard, Phys. Rev. B **77**, 214304 (2008).
10. S. Il Kim, K. Ahn, D.-H. Yeon, S. Hwang, H.-S. Kim, S. M. Lee, and K. H. Lee, Appl. Phys. Express **4**, 91801 (2011).
11. Z. Wanting, W. Hu, P. Wei, N. Xiaolei, and W. Zhao, J. Electron. Mater. **49**, 2962 (2020).
12. C. Li, S. Ma, P. Wei, W. Zhu, X. Nie, X. Sang, Z. Sun, Q. Zhang, and W. Zhao, Energy Environ. Sci. **13**, 535 (2020).
13. M. Gatti, F. Bruneval, V. Olevano, and L. Reining, Phys. Rev. Lett. **99**, 266402 (2007).
14. G. R. Khan and B. Ahmad, Appl. Phys. A **123**, 1 (2017).
15. K. S. Karimov, M. Mahroof-Tahir, M. Saleem, M. T. S. Chani, and A. K. Niaz, J. Semicond. **36**, 73004 (2015).
16. A. Paone, M. Joly, R. Sanjines, A. Romanyuk, J.-L. Scartezzini, and A. Schüler, in *Opt. Model. Meas. Sol. Energy Syst. III* (International Society for Optics and Photonics, 2009), p. 74100F.
17. I. Y. Forero-Sandoval, J. A. Chan-Espinoza, J. Ordonez-Miranda, J. J. Alvarado-Gil, F. Dumas-Bouchiat, C. Champeaux, K. Joulain, Y. Ezzahri, J. Drevillon, and C. L. Gomez-Heredia, Phys. Rev. Appl. **14**, 34023 (2020).
18. I. Kosta, C. Navone, A. Bianchin, E. García-Lecina, H. Grande, H. I. Mouko, J. Azpeitia, and I. García, J. Alloys Compd. **856**, 158069 (2021).
19. S. Y. Back, J. H. Yun, H. Cho, G. Kim, and J.-S. Rhyee, Materials (Basel). **14**, 2506 (2021).
20. G. Chen, *Nanoscale Energy Transport and Conversion: A Parallel Treatment of Electrons, Molecules, Phonons, and Photons* (Oxford university press, 2005).
21. F. J. Morin, Phys. Rev. Lett. **3**, 34 (1959).
22. J. Jung, S. Lee, B. Ryu, and S. Ryu, Int. J. Heat Mass Transf. **144**, 118620 (2019).
23. L. Qiu, Y. Du, Y. Bai, Y. Feng, X. Zhang, J. Wu, X. Wang, and C. Xu, J. Therm. Sci. **30**, 465 (2021).
24. J. Ordonez-Miranda, Y. Ezzahri, K. Joulain, J. Drevillon, and J. J. Alvarado-Gil, Phys. Rev. B **98**, 1 (2018).
25. L. Wang, L. Zhao, Z. Jiang, G. Luo, P. Yang, X. Han, X. Li, and R. Maeda, AIP Adv. **9**, 95067 (2019).
26. S. Alvarez-Guerrero, J. Ordonez-Miranda, R. de Coss, and J. J. Alvarado-Gil, Int. J. Therm. Sci. **172**, 107278 (2022).
27. F. Nilsson, J. Krueckel, D. W. Schubert, F. Chen, M. Unge, U. W. Gedde, and M. S.

Hedenqvist, Compos. Sci. Technol. **132**, 16 (2016).
28. J. Ordonez-Miranda, J. M. Hill, K. Joulain, Y. Ezzahri, and J. Drevillon, J. Appl. Phys. **123**, 1 (2018).
29. L. Qiu, N. Zhu, Y. Feng, E. E. Michaelides, G. Żyła, D. Jing, X. Zhang, P. M. Norris, C. N. Markides, and O. Mahian, Phys. Rep. **843**, 1 (2020).
30. L. Qiu, X. Zhang, Z. Guo, and Q. Li, Carbon N. Y. **178**, 391 (2021).
31. S. Jasmee, G. Omar, S. S. C. Othaman, N. A. Masripan, and H. A. Hamid, Polym. Compos. (2021).
32. H. Kizuka, T. Yagi, J. Jia, Y. Yamashita, S. Nakamura, N. Taketoshi, and Y. Shigesato, Jpn. J. Appl. Phys. **54**, (2015).
33. D. W. Oh, C. Ko, S. Ramanathan, and D. G. Cahill, Appl. Phys. Lett. **96**, (2010).
34. J. K. Chen, X. L. Liu, X. Yuan, Y. L. Zhang, Y. F. Gao, Y. F. Zhou, R. H. Liu, L. D. Chen, and N. F. Chen, Chinese Sci. Bull. **57**, 3393 (2012).
35. R. Kothari, C. T. Sun, R. Dinwiddie, and H. Wang, Int. J. Heat Mass Transf. **66**, 823 (2013).
36. A. Gupta, R. Singhal, J. Narayan, and D. K. Avasthi, J. Mater. Res. **26**, 2901 (2011).
37. Z. Yang, C. Ko, V. Balakrishnan, G. Gopalakrishnan, and S. Ramanathan, Phys. Rev. B **82**, 205101 (2010).
38. K. Ulutas, D. Deger, and S. Yakut, in *J. Phys. Conf. Ser.* (IOP Publishing, 2013), p. 12040.
39. H. Shang, C. Dun, Y. Deng, T. Li, Z. Gao, L. Xiao, H. Gu, D. J. Singh, Z. Ren, and F. Ding, J. Mater. Chem. A **8**, 4552 (2020).
40. E. Bin Kim, P. Dharmaiah, K.-H. Lee, C.-H. Lee, J.-H. Lee, J.-K. Yang, D.-H. Jang, D.-S. Kim, and S.-J. Hong, J. Alloys Compd. **777**, 703 (2019).
41. S. Parsamehr, A. Boochani, M. Amiri, S. Solaymani, E. Sartipi, S. Naderi, and A. Aminian, Philos. Mag. **101**, 369 (2021).
42. M. Ilkhani, A. Boochani, M. Amiri, M. Asshabi, and D. P. Rai, Solid State Commun. **308**, 113838 (2020).
43. R. Pöttgen, T. Jüstel, and C. A. Strassert, *Rare Earth Chemistry* (Walter de Gruyter GmbH & Co KG, 2020).
44. S. Il Kim, S. Hwang, J. W. Roh, K. Ahn, D.-H. Yeon, K. H. Lee, and S. W. Kim, J. Mater. Res. **27**, 2449 (2012).
45. C. Kittel, P. and P. McEuen, *Introduction to Solid State Physics* (Wiley New York, 1996).
46. S. Lee, K. Hippalgaonkar, F. Yang, J. Hong, C. Ko, J. Suh, K. Liu, K. Wang, J. J. Urban, and X. Zhang, Science (80-.). **355**, 371 (2017).
47. L. Jin, S. E. Zeltmann, H. S. Choe, H. Liu, F. I. Allen, A. M. Minor, and J. Wu, Phys. Rev. B **102**, 41120 (2020).